The Interactive Relationship between Air Travel and Climate

Kristopher B. Karnauskas *, Jeffrey P. Donnelly, Hannah C. Barkley

Woods Hole Oceanographic Institution, Woods Hole, MA

Jonathan E. Martin

University of Wisconsin, Madison, WI

* Corresponding author: kk@whoi.edu

Manuscript submitted to *Nature Climate Change*

July 14, 2014

The airline industry closely monitors the midlatitude jet stream for short term planning of flight paths and arrival times. In addition to passenger safety and on-time metrics, this is due to the acute sensitivity of airline profits to fuel cost and consumption. U.S. carriers spent $47 billion on jet fuel in 2011 [i], compared to a total industry operating revenue of $192 billion [ii]. Beyond the time scale of synoptic weather, the El Nino-Southern Oscillation (ENSO) and Arctic Oscillation (AO) modulate the strength and position of the Aleutian low and Pacific high on interannual time scales, which influence the tendency of the exit region of the midlatitude Pacific jet stream to extend, retract, and meander poleward and equatorward [1-3]. The impact of global aviation on climate change has been studied for decades due to the radiative forcing of emitted greenhouse gases, contrails, and other effects [4,5]. The impact of climate variability on air travel, however, has only recently come into focus and primarily in terms of turbulence [6,7]. Shifting attention to flight durations, here we show that 88% of the interannual variance in domestic flight durations over the Pacific sector is explained by a linear combination of ENSO and the AO. Further, we extend our analysis to CMIP5 model projections to quantify and discuss a new feedback to anthropogenic climate change.

The northeastern subtropical Pacific between Hawaii and the U.S. mainland is a major corridor of long-distance commercial air travel. Flying times [iii] between Honolulu (HNL) and Los Angeles (LAX), San Francisco (SFO), and Seattle–Tacoma (SEA) from 1995 through 2013 by four major carriers (United Airlines [UA], American Airlines [AA], Delta Airlines [DL], and Hawaiian Airlines [HA]) are analyzed and compared with observed [8] daily zonal winds at roughly cruising altitude (300 mb) (Fig. 1a). To isolate the signal associated with atmospheric variability (as opposed to systematic changes in traffic, technology or policy), rather than analyzing flying times in one direction or the other, the *difference* between westbound and eastbound flying times (ΔT) of each route is computed. There is substantial seasonal-to-interannual variability of ΔT (~1 hour), which is remarkably consistent between airlines and across routes (Fig. 1b). For example, the ΔT records for the HNL-LAX route exhibit correlations of 0.91 (DL vs. HA) to 0.95 (UA vs. DL). ΔT records for a given route are also significantly correlated with other routes for the same airline; the HNL-LAX route is correlated 0.86 with HNL-SFO, and HNL-SFO is correlated 0.65 with HNL-SEA. Moreover, correlations are very high between HNL-LAX and additional routes that extend well onto the continent: 0.81 for HNL-DEN (Denver), 0.82 for HNL-DFW (Dallas-Fort Worth), 0.75 for HNL-ORD (Chicago O'Hare), and 0.73 for HNL-ATL (Atlanta).

That the observed fluctuations in flying times are synchronous throughout the region regardless of airline or route suggests a common driver, which we hypothesize to be internal climate variability. Correlations of observed atmospheric anomalies with a representative ΔT record (UA HNL-LAX; mean seasonal cycle also removed) reveals the dominant large-scale mechanism. ΔT is anomalously large (*i.e.*, eastbound flights are shorter and westbound flights are longer) when the 300-mb westerly wind between Hawaii and the mainland is anomalously strong (Fig. 2a). Zonal wind correlations of opposite sign immediately poleward and equatorward are a clear manifestation of a cyclonic (anticyclonic) tropospheric circulation anomaly poleward (equatorward) of the airline route (Fig. 2b). This pattern of upper-level zonal wind and mid-tropospheric geopotential height is consistent with the leading modes of Pacific jet stream variability recently identified [9], and project strongly onto those of ENSO (El Nino phase) and the AO (negative phase) (Fig. S1).

To facilitate analysis of the observed temporal covariability of 300-mb zonal wind and ΔT, an index is constructed as the spatially averaged 300-mb zonal wind between Hawaii and the U.S. mainland (u_{300mb}; box shown in Fig. 2a). The mean seasonal cycle of u_{300mb} explains virtually all of the mean seasonality of flying time between Los Angeles and Honolulu (r=0.98; Fig. S2), with similar results for the other routes. The correlations between u_{300mb} and ΔT are very high across all time scales down to the highest frequency fluctuations associated with synoptic weather variability (Fig. 3a). After removing the mean seasonal cycle of both data sets, u_{300mb} explains 73% of the total daily variance of ΔT and 91% of the interannual variance. Thus, the atmosphere's well-known influence on aviation readily transcends from weather to climate scales.

The 19-year records of observed u_{300mb} (and thus ΔT) share substantial variance with large-scale modes of tropical and high-latitude climate variability, particularly ENSO and the AO (Fig. 3c). For example, the largest positive anomalies are coincident with major El Nino events (including 1997-98 and 2009-10), while the leveling off at the peak of such anomalies is akin to the AO record. The interannual variability of ΔT is correlated 0.91 with ENSO at a 2-3 month lag, and -0.48 with the AO (no significant lag). Indeed, a simple least squares multiple linear regression using the NINO3.4 and AO indices as independent variables is able to capture 82% of the variance of the observed $u300_{mb}$ index – 88% (r=0.94) if NINO3.4 is allowed to lead by 60 days (Fig. 3d). It is highly plausible that propagating modes of intraseasonal variability such as the Madden-Julian Oscillation (MJO) also have a strong impact on air travel in this region, particularly at higher frequencies than those shown in Fig. 3c-d.

Although the relationship between the durations of westbound and eastbound legs of a given route is inverse and strong, careful analysis of the total flying time by route (westbound leg plus eastbound leg; *ΣT*) reveals a small but nonzero residual (Fig. S3) [iv]. This implies that changes in flying times and thus fuel consumption, CO_2 emissions, *etc.* do not entirely cancel out as 300-mb zonal winds change either as part of internal, oscillatory atmospheric variability or in response to radiative forcing. In 2011, U.S. carriers purchased jet fuel at ~$3 per gal [v]. There are ~30,000 U.S. domestic flights per day [vi]. Assuming each flight has a counterpart in the opposite direction, there are 15,000 individual routes flown per day. If the total flying time by route (*ΣT*) increased by just one minute for every route, there would be a total of 250 additional flying hours per day, or ~91,000 additional flying hours per year, spelling potentially billions of additional dollars spent on jet fuel and a significant increase in the contribution to global radiative forcing by the airline industry. It is therefore essential, as a matter of understanding feedbacks between climate and society, to characterize and understand the response of the 300-mb wind field to radiative forcing.

Analyzing the predicted response of 300-mb zonal winds to increased radiative forcing by 34 GCMs included in the Coupled Model Intercomparison Project, Phase 5 (CMIP5) [10] paints an uncertain future (Fig. 4a). Under the 8.5 W m^{-2} IPCC forcing experiment (RCP8.5), roughly one third of GCMs predict a poleward shift of the annual mean position of the jet (Fig. 4c), one fifth predict an equatorward shift (Fig. 4d), and the remaining half predict only a very small or insignificant change in the latitudinal position or strength of the annual mean jet. However, the most robust aspect of the projected change in the annual mean 300-mb zonal wind field over the North Pacific – consistent across half of the GCMs – is a zonal extension of the jet exit region into the corridor between Hawaii and the U.S. mainland (1.6 ± 0.4 m s^{-1} local increase in mean annual 300-mb zonal wind [u_{300mb} index]) (Fig. 4e). The multi-model ensemble projections shown in Fig. 4 based on CMIP5 models are highly consistent with a previous assessment of

CMIP3 models [11,12] and further underscore the importance of GCMs to reliable predict the future state of the tropical Pacific Ocean. Based on the observed empirical relationships discussed above, such a change in upper level winds would result in ~3.7 additional flying hours per daily round-trip, per carrier, per comparable route, per year. Assuming twice-daily round-trip flights, four carriers, and just three comparable routes (*i.e.*, HNL to/from LAX, SFO, and SEA) yields 89 additional flying hours per year, which amounts to roughly 320,000 gal additional jet fuel consumed per year [vii], ~$1 million in additional fuel costs, and 3.1 million kg CO_2 emitted per year [viii]. Multi-model projections focusing on the boreal winter season (Dec.-Jan.), which is the season of maximum climatological jet development, are much larger and more robust across models (Fig. 4b). The multi-model median change in 300-mb zonal wind between Hawaii and the U.S. mainland (u_{300mb} index) during boreal winter is 5.0 ± 1.4 m s^{-1} (accounting for 69 additional flying hours, 247,000 gal additional jet fuel consumed, $741,000 additional fuel cost, and 2.4 million kg CO_2 emitted *per winter* under the same assumptions).

Given the observed dependence of flight durations on 300-mb zonal winds (Fig. 3), as germane to airline operations may be the level of *variability* of 300-mb winds– analogous to volatility in a market or in the price of raw materials. How is the amplitude of daily-scale (synoptic) variability of u_{300mb} modulated seasonally and interannually? How is the amplitude of lower-frequency variability (*i.e.*, the amplitude of the seasonal cycle and the magnitude of interannual anomalies) projected to change in the response to radiative forcing? It is well known that synoptic-scale weather variability is significantly more energetic during wintertime (Fig. 5a); so, too, is the daily-scale variability in flying times (Fig. 5b). At the interannual time scale, the daily-scale variance in u_{300mb} also proves to be modulated by the phase of the AO; the variance of u_{300mb} is anomalously large when the AO is in a negative phase (Fig. 5c, d). IPCC syntheses of GCM projections include a trend toward the positive phase of the AO over the course of this century in response to radiative forcing [4,13], implying that the 300-mb zonal winds in this region may become less variable on a day-to-day basis in the future. However, the annual cycle of u_{300mb} is projected to become stronger under the RCP8.5 forcing experiment (Fig. 5e), which is consistent with the projected trend in u_{300mb} being greatest during boreal winter– the season of maximum climatological u_{300mb} (Fig. 5g, h). The CMIP5 projections analyzed herein do not include a robust change in the amplitude of interannual variability of u_{300mb} (Fig. 5f), which is also consistent with IPCC syntheses noting the lack of robust changes in the amplitude of ENSO and AO.

It is clear that the acute sensitivity of the commercial airline industry to atmospheric variability extends beyond "weather"– to the seasonal and interannual ("climate") time scales. Synoptic weather patterns, the annual cycle of solar forcing, and modes of interannual climate variability such as ENSO and the AO control the strength and variance of flight level winds, and flight level winds appear to be the overwhelmingly dominant predictor of flight durations. Climate mechanisms that dictate the variability of flight durations in other busy regions such as the North Atlantic, Europe, and Asia are likely to differ in details from those identified herein but still probably boil down to what controls flight level winds between airports. While much of the discussion of the relationship between climate change and air travel focuses on the contribution of global aviation to radiative forcing (greenhouse gases and contrails), the findings presented herein suggest more complex feedbacks. In particular, radiatively forced changes in circulation have the potential to influence the rate of consumption of fossil fuels by the airline industry, thus feeding back onto the global radiative forcing and resultant changes in circulation.

Figure Legends

Figure 1 | Overview map and airline time series. **a**, Airline routes between Honolulu (HNL) and Los Angeles (LAX), San Francisco (SFO), and Seattle-Tacoma (SEA) International Airports superimposed upon the annual mean 300-mb zonal wind field (NCEP/NCAR Reanalysis, 1995-2013). The zonal wind field is contoured every 2.5 m s^{-1}. **b**, Time series of the flying time differences between westbound and eastbound legs (ΔT) for the HNL-SEA, HNL-SFO, and HNL-LAX routes. Colors in each panel of **b** denote airline (blue for United, red for American, green for Delta, and cyan for Hawaiian). A 31-day running mean was applied to all time series. No HNL-SEA data were available from United or American.

Figure 2 | Atmospheric correlations. Anomaly correlation of the **a**, 300-mb zonal wind and **b**, 500-mb geopotential height fields with the flying time difference between westbound and eastbound legs (ΔT) for the HNL-LAX route based on United flights. The mean seasonal cycle was removed from– and a 31-day running mean was applied to all data. For reference, the annual mean 300-mb zonal wind and 500-mb geopotential height fields are also contoured in black (every 2 m s^{-1} beginning at 5 m s^{-1} and every 50 m beginning at 5,000 m, respectively). The box shown in **a** indicates the region over which 300-mb zonal wind field is spatially averaged to construct the u_{300mb} index.

Figure 3 | Flying time, wind, and climate. **a**, Daily, **b**, monthly and **c**, annually smoothed HNL-LAX (United) flying time difference (ΔT; blue) and u_{300mb} index (black). The u_{300mb} index is defined as the spatially averaged 300-mb zonal wind over the box shown in Fig. 2a. The inset to **a** shows daily ΔT and u_{300mb} time series for the year 2009. u_{300mb} vs. ΔT correlation coefficients associated with daily, monthly, and annually smothed time series are 0.86, 0.91, and 0.95, respectively. Also shown in **c** are annually smoothed NINO3.4 (dark gray) and AO (light gray;

inverted) climate indices. Correlations associated with NINO3.4 are 0.86 and 0.85 for u_{300mb} and ΔT, respectively (the maximum lead-lag correlation of NINO3.4 and ΔT is 0.91 with NINO3.4 leading by ~2.5 months). Correlations associated with the AO are -0.53 and -0.48 for u_{300mb} and ΔT, respectively. **d**, Observed (gray) and reconstructed (black) annually smoothed u_{300mb} index based on least-squares multiple linear regression with the NINO3.4 (leading by 60 days) and AO indices as independent variables.

Figure 4 | Projected trends in mean flight level winds. **a**, CMIP5 multi-model (N=34) mean trend in 300-mb zonal wind under the IPCC AR5 RCP8.5 future forcing experiment (2006-2100). For reference, the multi-model, annual mean 300-mb zonal wind field is also contoured in black (every 5 m s^{-1} beginning at 5 m s^{-1}). **b**, As in **a** but for the boreal winter season (Dec.-Jan.). **c**, As in **a** but including only those models that predict a northward shift of the Pacific jet stream (N=13). **d**, As in **a** but including only those models that predict a southward shift of the Pacific jet stream (N=6). **e**, As in **a** but including only those models that predict a pronounced southward dip of the Pacific jet stream (N=17). The inset in **b** shows a histogram of projected trends in 300-mb zonal wind spatially averaged over the box shown (*i.e.*, the u_{300mb} index). The solid and dashed vertical lines represent zero and the median projected u_{300mb} trend, respectively.

Figure 5 | Changes in variability. **a**, Observed daily-scale u_{300mb} for 1995-1999 (to show detail). Daily-scale is defined as the departure from the 7-day running mean. **b**, as in **a** but for the flying time from LAX to HNL (United). **c**, Annually smoothed AO index (inverted). **d**, Annually smoothed 90-day running variance of daily-scale u_{300mb}. **e**, Histogram of CMIP5 projected trends in 10-year running variance of monthly u_{300mb} under the IPCC AR5 RCP8.5 future forcing experiment (2006-2100). **f**, As in **e** but for monthly u_{300mb} anomalies (mean seasonal cycle removed). **g**, Mean seasonal cycle of u_{300mb} in CMIP5 models (thin lines) and the multi-model mean (thick line). **h**, Projected trends in u_{300mb} by CMIP5 models as a function of calendar month (thin lines) and the multi-model mean (thick line).

Figure S1 | ENSO and Arctic Oscillation. Regression of Northern Hemisphere wintertime **a**, 300-mb zonal wind (m s^{-1}) and **b**, 500-mb geopotential height (m) on the NINO3.4 index from the NCEP/NCAR Reanalysis (1949-2010). **c**, **d**, As in **a**, **b** but for the the Arctic Oscillation (AO) index.

Figure S2 | Annual cycles. a, Annual cycle of westbound (blue) and eastbound (red) flying time (*T*) between HNL and LAX (United). **b**, Annual cycle of the flying time difference between westbound and eastbound legs (ΔT) for the HNL-LAX route (United). **c**, As in **b** but for the flight time sum. **d**, Annual cycle of the u_{300mb} index.

Figure S3 | Flight time residual. a, Scatter diagram of the u_{300mb} index vs. the duration of westbound (blue) and eastbound (red) legs of the HNL-LAX route (United). **b**, As in **a** but for the u_{300mb} index vs. the flight time sum.

Corresponding Author Kristopher B. Karnauskas. Woods Hole Oceanographic Institution, 360 Woods Hole Road, M.S. 23, Woods Hole, Massachusetts 02543, USA. *e-mail: kk@whoi.edu.

Acknowledgements The authors thank B. Carmichael and B. Sharman of the National Center for Atmospheric Research Aviation Applications Program, G. Compo of the Cooperative Institute for Research in the Environmental Sciences, and D. Battisti of the University of Washington Department of Atmospheric Sciences for helpful discussions. We acknowledge the World Climate Research Programme's Working Group on Coupled Modelling, which is responsible for CMIP5, and we thank the climate modeling groups for producing and making available their model output. For CMIP5, the U.S. Department of Energy's Program for Climate Model Diagnosis and Intercomparison provides coordinating support and led development of software infrastructure in partnership with the Global Organization for Earth System Science Portals. CMIP5 model output data acquired via the WHOI CMIP5 Community Storage Server, Woods Hole Oceanographic Institution, Woods Hole, MA, USA from their website at http://cmip5.whoi.edu/ (WHOI internal use only). NCEP/NCAR Reanalysis data provided by the NOAA/OAR/ESRL PSD, Boulder, Colorado, USA, from their Web site at http://www.esrl.noaa.gov/psd/. K.B.K. acknowledges support from the Strategic Environmental Research and Development Program, the WHOI Oceans and Climate Change Institute, and the Alfred P. Sloan Foundation.

Author Contributions K.B.K. and H.C.B. jointly conceived the study. K.B.K. conducted the analyses and wrote the paper with input from all authors.

Additional Information The authors declare no competing financial interests. Reprints and permissions information is available online at www.nature.com/reprints. Correspondence and requests for materials should be addressed to K.B.K.

References

1. Horel, J. D. & Wallace, J. M. Planetary-Scale Atmospheric Phenomena Associated with the Southern Oscillation. *Mon Weather Rev* **109**, 813-829, doi:Doi 10.1175/1520-0493(1981)109<0813:Psapaw>2.0.Co;2 (1981).
2. Seager, R., Harnik, N., Kushnir, Y., Robinson, W. & Miller, J. Mechanisms of hemispherically symmetric climate variability. *J Climate* **16**, 2960-2978, doi:Doi 10.1175/1520-0442(2003)016<2960:Mohscv>2.0.Co;2 (2003).
3. Thompson, D. W. J. & Wallace, J. M. Annular modes in the extratropical circulation. Part I: Month-to-month variability. *J Climate* **13**, 1000-1016, doi:Doi 10.1175/1520-0442(2000)013<1000:Amitec>2.0.Co;2 (2000).
4. Solomon, S., Intergovernmental Panel on Climate Change. & Intergovernmental Panel on Climate Change. Working Group I. *Climate change 2007 : the physical science basis : contribution of Working Group I to the Fourth Assessment Report of the Intergovernmental Panel on Climate Change*. (Cambridge University Press, 2007).
5. Burkhardt, U. & Karcher, B. Global radiative forcing from contrail cirrus. *Nat Clim Change* **1**, 54-58, doi:Doi 10.1038/Nclimate1068 (2011).
6. Williams, P. D. & Joshi, M. M. Intensification of winter transatlantic aviation turbulence in response to climate change. *Nat Clim Change* **3**, 644-648, doi:Doi 10.1038/Nclimate1866 (2013).
7. Wolff, J. K. & Sharman, R. D. Climatology of upper-level turbulence over the contiguous united states. *J Appl Meteorol Clim* **47**, 2198-2214, doi:Doi 10.1175/2008jamc1799.1 (2008).

8 Kalnay, E. *et al.* The NCEP/NCAR 40-year reanalysis project. *B Am Meteorol Soc* **77**, 437-471, doi:Doi 10.1175/1520-0477(1996)077<0437:Tnyrp>2.0.Co;2 (1996).

9 Jaffe, S. C., Martin, J. E., Vimont, D. J. & Lorenz, D. J. A Synoptic Climatology of Episodic, Subseasonal Retractions of the Pacific Jet. *J Climate* **24**, 2846-2860, doi:Doi 10.1175/2010jcli3995.1 (2011).

10 Taylor, K. E., Stouffer, R. J. & Meehl, G. A. An Overview of Cmip5 and the Experiment Design. *B Am Meteorol Soc* **93**, 485-498, doi:Doi 10.1175/Bams-D-11-00094.1 (2012).

11 Delcambre, S. C., Lorenz, D. J., Vimont, D. J. & Martin, J. E. Diagnosing Northern Hemisphere Jet Portrayal in 17 CMIP3 Global Climate Models: Twenty-First-Century Projections. *J Climate* **26**, 4930-4946, doi:Doi 10.1175/Jcli-D-12-00359.1 (2013).

12 Delcambre, S. C., Lorenz, D. J., Vimont, D. J. & Martin, J. E. Diagnosing Northern Hemisphere Jet Portrayal in 17 CMIP3 Global Climate Models: Twentieth-Century Intermodel Variability. *J Climate* **26**, 4910-4929, doi:Doi 10.1175/Jcli-D-12-00337.1 (2013).

13 Stocker, T. F. & Change., I. P. o. C. *Climate change 2013 : the physical science basis : Working Group I contribution to the Fifth Assessment Report of the Intergovernmental Panel on Climate Change*.

Other Notes

---

[i] Bureau of Transportation Statistics, Research and Innovative Technology Administration, U.S. Department of Transportation.

[ii] MIT Global Airline Industry Program, Airline Data Project (http://web.mit.edu/airlinedata/www/Revenue&Related.html).

[iii] The BTS statistic "AirTime" is used, which is wheels up to wheels down.

[iv] The sensitivity of westbound flight durations to u_{300} is greater than that of eastbound flights of the same route, so an increase in u_{300} lengthens the westbound flight by slightly more than it shortens the eastbound flight resulting in a net increase in total flying time (ΣT). The average sensitivity of ΣT to u_{300} for the flights analyzed is 0.38 minutes flying time per m s^{-1} zonal wind.

[v] Bureau of Transportation Statistics, Research and Innovative Technology Administration, U.S. Department of Transportation.

[vi] National Air Traffic Controllers Association.

[vii] Assume burn rate 1 gal per second. Varies depending on aircraft and many other variables.

[viii] Assume emissions coefficient 9.6 kg CO_2 per gal (eia.gov/environment/emissions/co2_vol_mass.cfm).

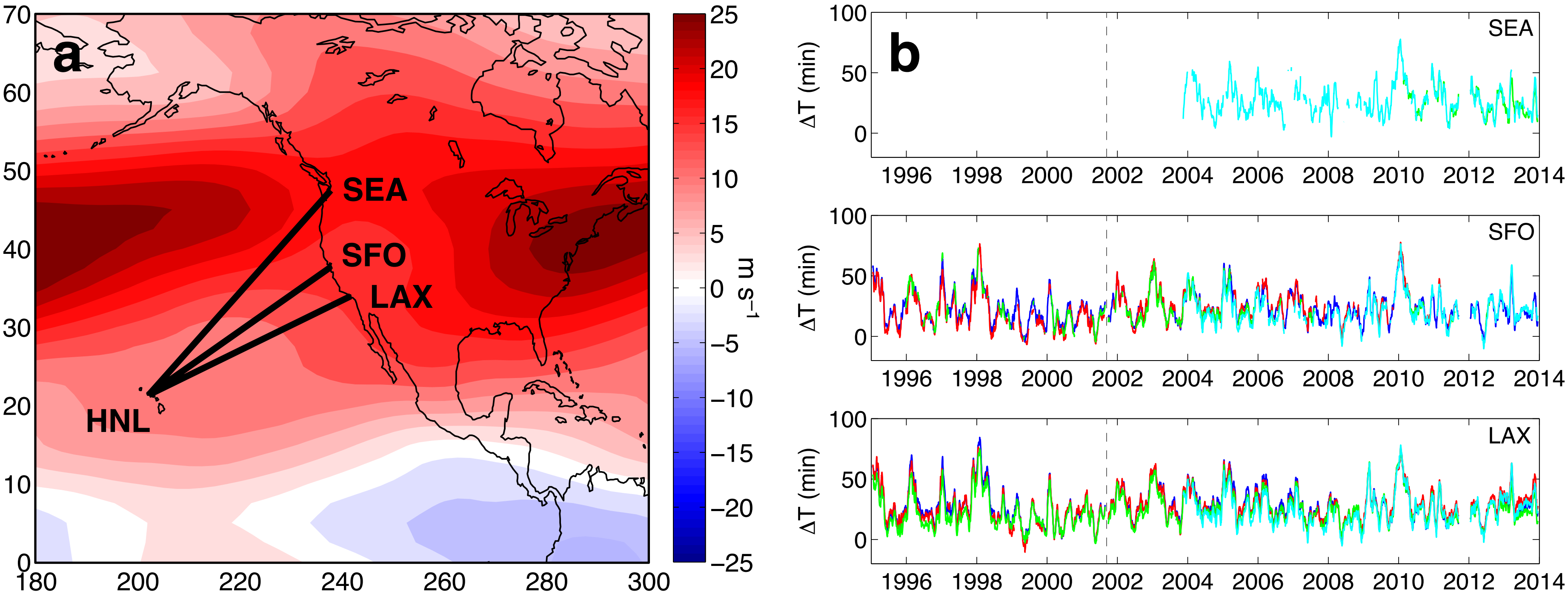

Figure 1 | Overview map and airline time series. a, Airline routes between Honolulu (HNL) and Los Angeles (LAX), San Francisco (SFO), and Seattle-Tacoma (SEA) International Airports superimposed upon the annual mean 300-mb zonal wind field (NCEP/NCAR Reanalysis, 1995-2013). The zonal wind field is contoured every 2.5 m s^{-1}. **b**, Time series of the flying time differences between westbound and eastbound legs (ΔT) for the HNL-SEA, HNL-SFO, and HNL-LAX routes. Colors in each panel of **b** denote airline (blue for United, red for American, green for Delta, and cyan for Hawaiian). A 31-day running mean was applied to all time series. No HNL-SEA data were available from United or American.

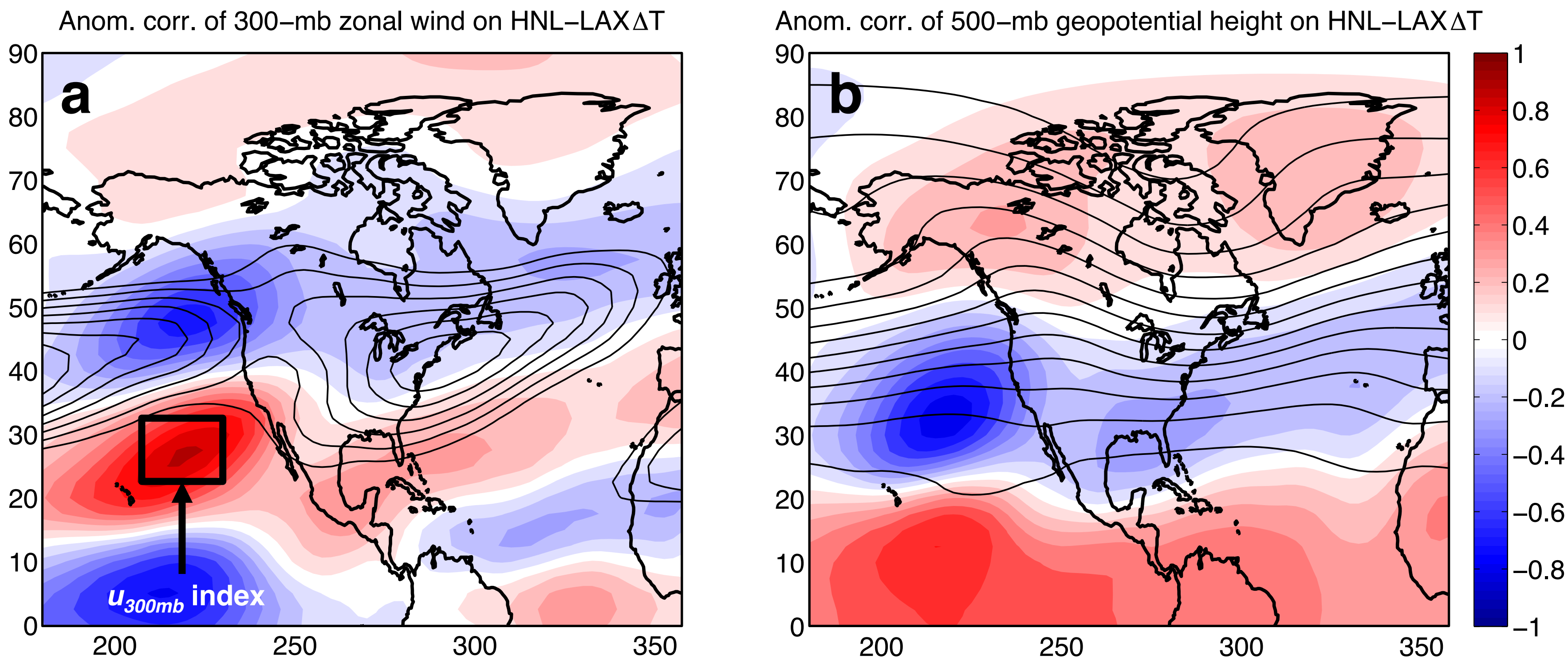

Figure 2 | Atmospheric correlations. Anomaly correlation of the **a**, 300-mb zonal wind and **b**, 500-mb geopotential height fields with the flying time difference between westbound and eastbound legs (*ΔT*) for the HNL-LAX route based on United flights. The mean seasonal cycle was removed from– and a 31-day running mean was applied to all data. For reference, the annual mean 300-mb zonal wind and 500-mb geopotential height fields are also contoured in black (every 2 m s^{-1} beginning at 5 m s^{-1} and every 50 m beginning at 5,000 m, respectively). The box shown in **a** indicates the region over which 300-mb zonal wind field is spatially averaged to construct the u_{300mb} index.

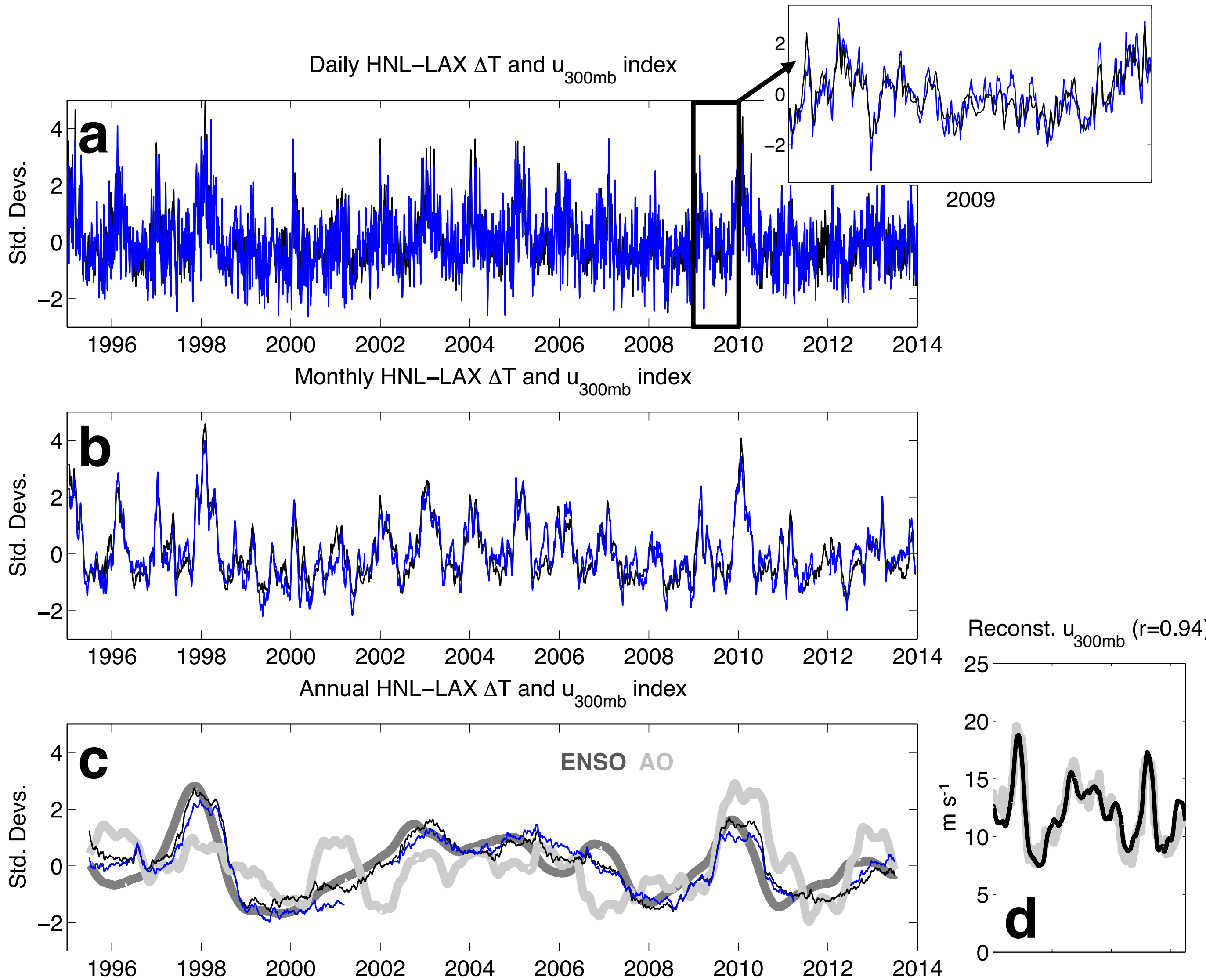

Figure 3 | Flying time, wind, and climate. a, Daily, **b**, monthly and **c**, annually smoothed HNL-LAX (United) flying time difference (ΔT; blue) and u_{300mb} index (black). The u_{300mb} index is defined as the spatially averaged 300-mb zonal wind over the box shown in Fig. 2a. The inset to **a** shows daily ΔT and u_{300mb} time series for the year 2009. u_{300mb} vs. ΔT correlation coefficients associated with daily, monthly, and annually smothed time series are 0.86, 0.91, and 0.95, respectively. Also shown in **c** are annually smoothed NINO3.4 (dark gray) and AO (light gray; inverted) climate indices. Correlations associated with NINO3.4 are 0.86 and 0.85 for u_{300mb} and ΔT, respectively (the maximum lead-lag correlation of NINO3.4 and ΔT is 0.91 with NINO3.4 leading by ~2.5 months). Correlations associated with the AO are -0.53 and -0.48 for u_{300mb} and ΔT, respectively. **d**, Observed (gray) and reconstructed (black) annually smoothed u_{300mb} index based on least-squares multiple linear regression with the NINO3.4 (leading by 60 days) and AO indices as independent variables.

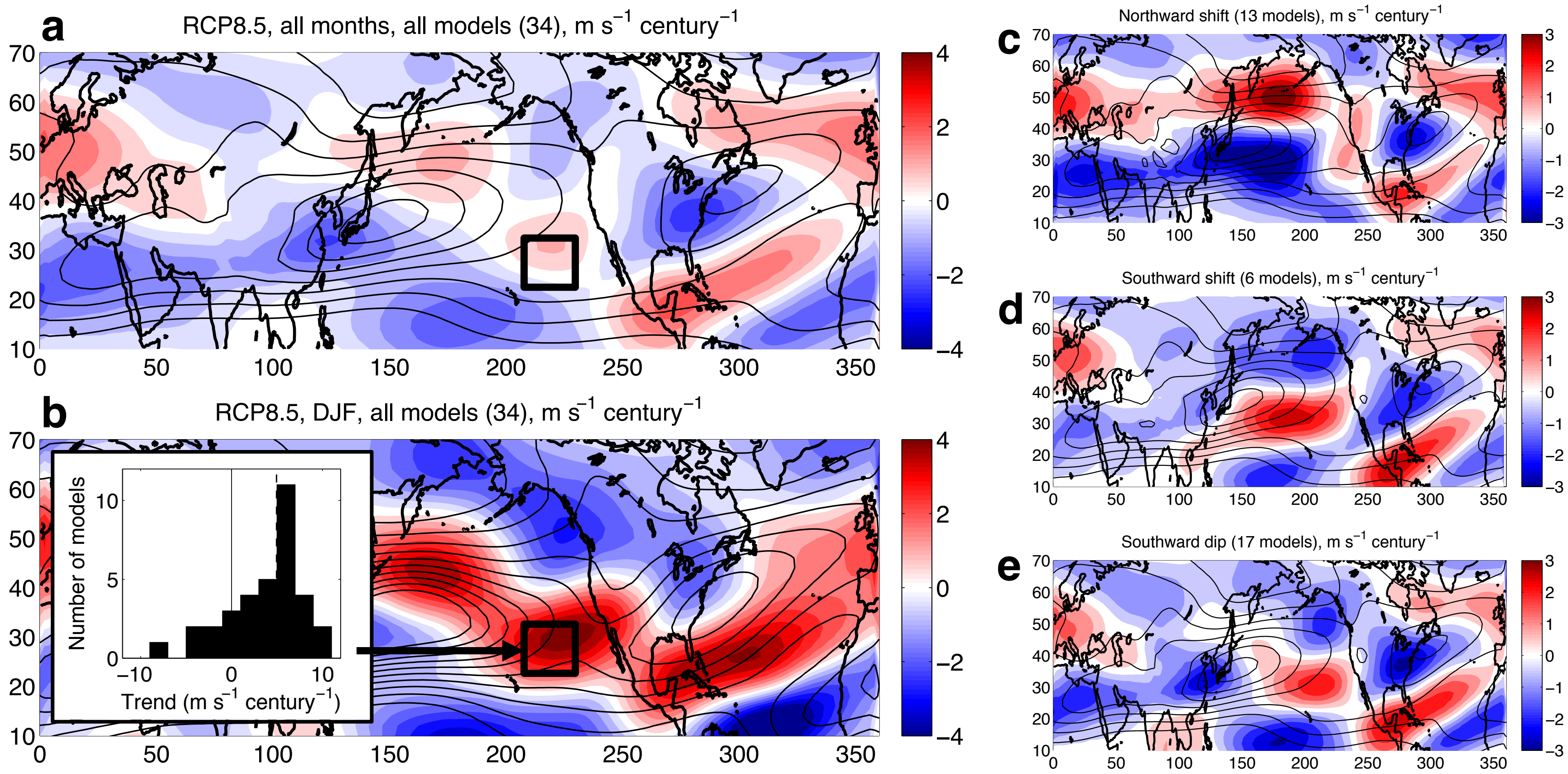

Figure 4 | Projected trends in mean flight level winds. **a**, CMIP5 multi-model (N=34) mean trend in 300-mb zonal wind under the IPCC AR5 RCP8.5 future forcing experiment (2006-2100). For reference, the multi-model, annual mean 300-mb zonal wind field is also contoured in black (every 5 m s^{-1} beginning at 5 m s^{-1}). **b**, As in **a** but for the boreal winter season (Dec.-Jan.). **c**, As in **a** but including only those models that predict a northward shift of the Pacific jet stream (N=13). **d**, As in **a** but including only those models that predict a southward shift of the Pacific jet stream (N=6). **e**, As in **a** but including only those models that predict a pronounced southward dip of the Pacific jet stream (N=17). The inset in **b** shows a histogram of projected trends in 300-mb zonal wind spatially averaged over the box shown (*i.e.*, the u_{300mb} index). The solid and dashed vertical lines represent zero and the median projected u_{300mb} trend, respectively.

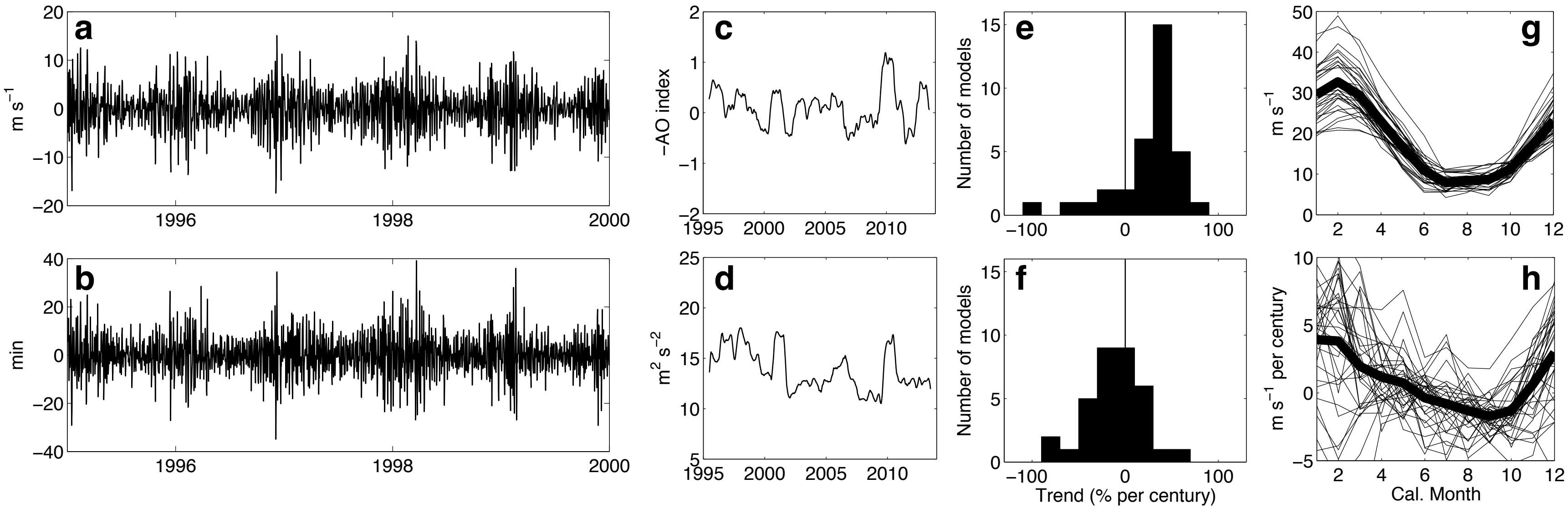

Figure 5 | Changes in variability. a, Observed daily-scale u_{300mb} for 1995-1999 (to show detail). Daily-scale is defined as the departure from the 7-day running mean. **b**, as in **a** but for the flying time from LAX to HNL (United). **c**, Annually smoothed AO index (inverted). **d**, Annually smoothed 90-day running variance of daily-scale u_{300mb}. **e**, Histogram of CMIP5 projected trends in 10-year running variance of monthly u_{300mb} under the IPCC AR5 RCP8.5 future forcing experiment (2006-2100). **f**, As in **e** but for monthly u_{300mb} anomalies (mean seasonal cycle removed). **g**, Mean seasonal cycle of u_{300mb} in CMIP5 models (thin lines) and the multi-model mean (thick line). **h**, Projected trends in u_{300mb} by CMIP5 models as a function of calendar month (thin lines) and the multi-model mean (thick line).

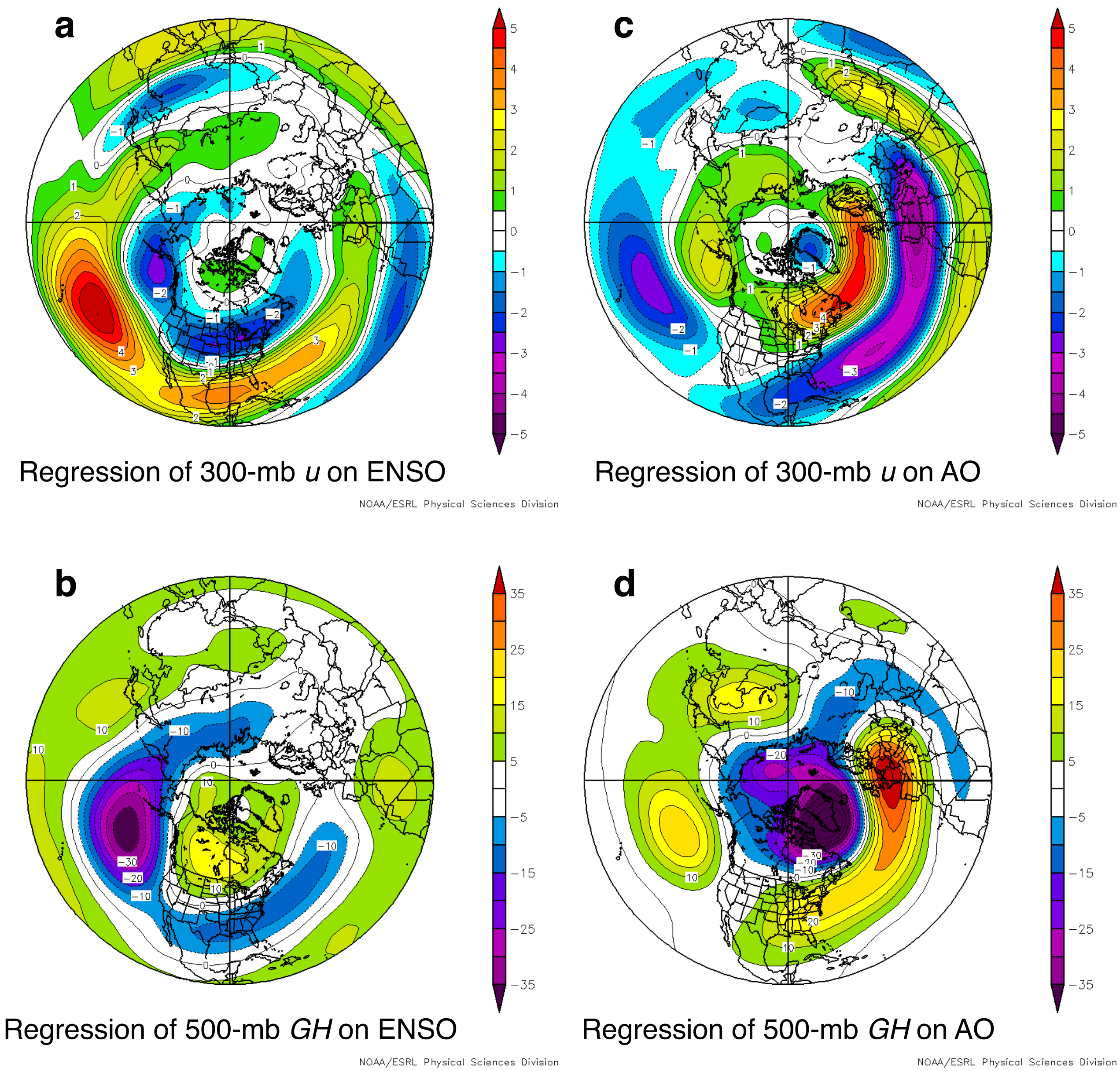

Figure S1 | ENSO and Arctic Oscillation. Regression of Northern Hemisphere wintertime **a**, 300-mb zonal wind ($m\ s^{-1}$) and **b**, 500-mb geopotential height (m) on the NINO3.4 index from the NCEP/NCAR Reanalysis (1949-2010). **c**, **d**, As in **a**, **b** but for the the Arctic Oscillation (AO) index.

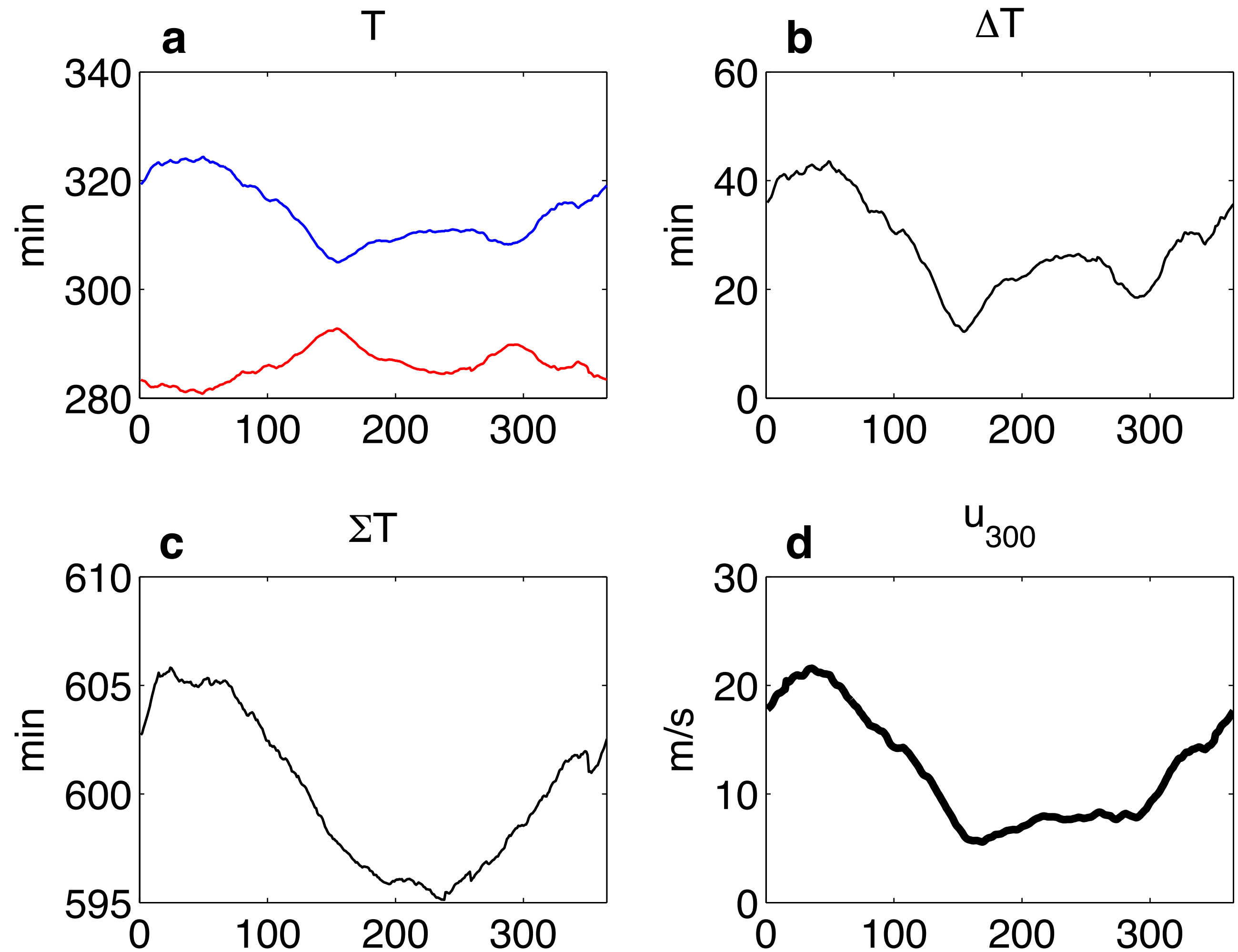

Figure S2 | Annual cycles. **a**, Annual cycle of westbound (blue) and eastbound (red) flying time (*T*) between HNL and LAX (United). **b**, Annual cycle of the flying time difference between westbound and eastbound legs (ΔT) for the HNL-LAX route (United). **c**, As in **b** but for the flight time sum. **d**, Annual cycle of the u_{300mb} index.

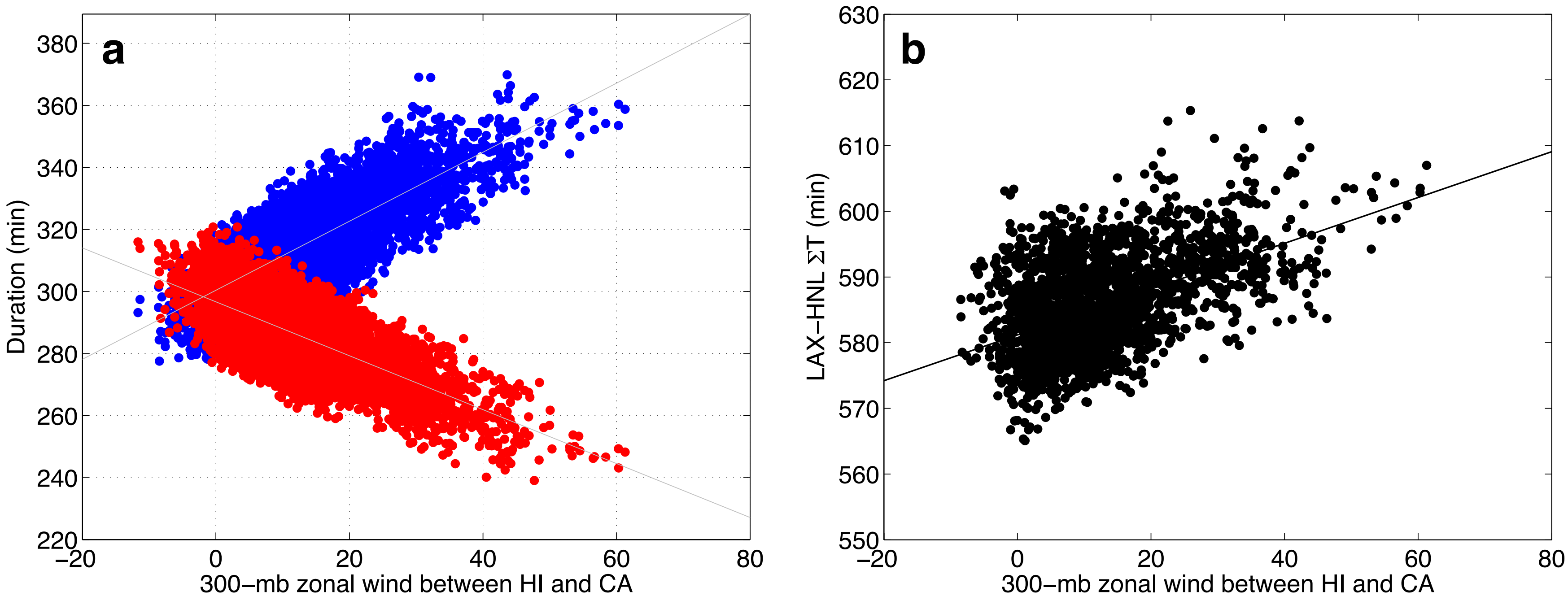

Figure S3 | Flight time residual. a, Scatter diagram of the u_{300mb} index vs. the duration of westbound (blue) and eastbound (red) legs of the HNL-LAX route (United). **b**, As in **a** but for the u_{300mb} index vs. the flight time sum.